Solid Freeform Fabrication 2022: Proceedings of the 33rd Annual International Solid Freeform Fabrication Symposium – An Additive Manufacturing Conference
Reviewed Paper

EFFECTS DUE TO VARIATIONS IN THERMAL PROPERTIES OF MARAGING STEEL FOR FINITE ELEMENT MODELING OF THE WAAM PROCESS

Matthew Register*† and Matthew W. Priddy*†

*Department of Mechanical Engineering, Mississippi State University, 210 Carpenter Hall, Mississippi State, MS 39762, USA
†Center for Advanced Vehicular Systems, 200 Research Blvd, Starkville, MS 39759, USA

Abstract

Finite element (FE) thermal simulations of the wire arc additive manufacturing (WAAM) process have been widely used to predict the temperature history of as-built parts. Temperature-dependent thermal properties like density, conductivity, specific heat, and latent heat are required to accurately simulate the solidus to liquidus transition seen in the heat affected zone. Current research has shown that thermal properties measured experimentally or simulated using material database software can be used for thermal modeling; however, there has been no direct comparison shown to determine which is most appropriate for WAAM modeling. The focus of this research is to compare the temperature variation of the FE thermal simulations with experimentally measured and computer-generated properties for M250 grade maraging steel. The thermal history for thin wall builds are compared with differing temperature-dependent thermal properties to examine the relationship between thermal properties and history. It was shown that constant values at room temperature result in an increased thermal response for WAAM thermal simulations and linearized properties decreased the temperature when both were compared with the experimental thermal property inputs. Further work needs to be performed before determining the most appropriate source for thermal properties (wrought, wire, as-built, or material database), but it can be concluded that the form of material does affect the thermal response for maraging grade 250 steel.

Introduction and Background

Wire arc additive manufacturing (WAAM) is a metal based additive manufacturing (AM) technology used to produce large near net shape parts [1], [2]. The process utilizes in the form of an arc to melt wire feedstock in a layer-by-layer fashion [3], [4]. Standard welding equipment is often used such as gas metal arc welding, gas tungsten arc welding, or plasma arc welding. WAAM has been an increasing area of research in AM due to its high deposition rates and material efficiency compared to other metal AM processes like laser powder bed fusion [1], [3], [5]. With deposition rates up to 10 kg/hr [5], it can be used to manufacture large components in a reasonable time compared to traditional casting methods. However, parts manufactured using WAAM often experience challenges caused by the large heat input and thermal cycling introduced into the part during printing.

Repeated heating and cooling cycles during the printing process leads to non-uniform thermal expansion and contraction of the material inducing residual stresses and part distortion [1], [6]. The WAAM process is intended for large-scale parts; however, with increased part size there is a greater chance of geometric inaccuracies due to a reduction in cooling rate as the part height increases [7]. As a result, the accuracy of the thermal history of a printed part is essential in determining the resultant microstructure, mechanical properties, and geometrical accuracy [8]. FE analysis can be used to predict the temperature history and residual stress of the WAAM process before building the part experimentally, saving time and labor costs [9]–[13].

The FE thermal simulation requires the use of temperature dependent thermal conductivity, specific heat, and latent heat of fusion; however, there has been little evidence supporting which source is best for these properties regarding WAAM simulations. Additionally, temperature dependent thermal properties can be very difficult to find in literature depending on the amount of research on the material of interest. In literature, properties which cannot be found are often generated by input of the elemental composition into a material database software [14], [15]. Constant property values associated with room temperature (RT) have also been used as oversimplifications when the properties cannot be found in literature [16]. Experimentally measured

values can be collected using digital scanning calorimetry (DSC) and laser flash technique (LFA);however, this can be costly and time consuming [17], [18]. To add to this variety, the properties can be gathered across a large range of temperatures from RT to well above the melting temperature. Lastly, it is unclear how the material state could play a role in thermal response. For example, the filler wire used for the welding process may result in thermal properties that differ from wrought or as-built material.

This paper investigates the variability in temperature history associated with variety of the thermal property inputs in a FE WAAM simulation using Abaqus/Standard 2019. Temperature dependent properties investigated include thermal conductivity, specific heat, and latent heat of fusion for filler wire and as-built material. Maraging grade 250 (M250) was chosen as the material of interest due to its excellent weldability and mechanical strength [19]. Several cases were tested including the actual measured values determined by DSC and LFA, constant values at RT, and linearized properties. The nodal temperature was simulated for a WAAM thin wall build, and values were measured at the center of the part on the top surfaces of layers 0, 1, 5, and 10 to best understand how various thermal property inputs can affect the temperature history in the part.

Materials and Methodology

Experimental Build Details

A 10-layered thin wall was built with a 1.1 mm diameter M250 wire using a Fronius TPS 4000 Cold Metal Transfer (CMT) Advanced Welding Package. The material used for the substrate was A36 mild steel. Machine data was recorded throughout the deposition process to be used later for the simulation to accurately match the experimental conditions. The gathered data includes voltage, current, travel speed, x, y, z coordinate locations, and arc activation. The printing process parameters used are listed in **Table 1.**

Table 1. The WAAM process parameters used during the build.

Current [A]	Voltage [V]	Power [W]	Travel Speed [mm/s]	Wire Feed Speed [in/min]
160	15	2400	10	250

With this information, the print path was modeled precisely to match the experimental setup. During the deposition process, four thermocouples (type K, size 0.032” Omega model KMQXL-032U-24) were used to measure the temperature variation over time. The locations of each thermocouple can be seen in **Figure 1**.

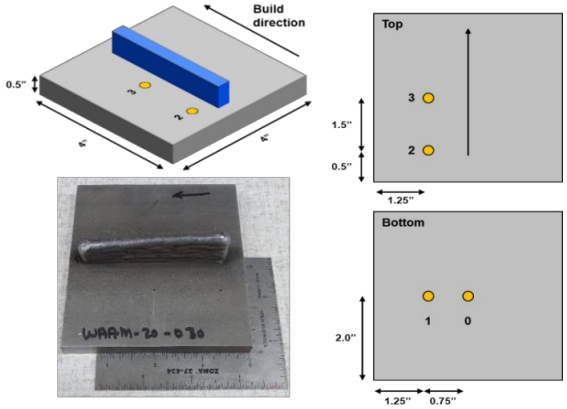

Figure 1. The CAD drawing for the thin wall (top left), the built part (bottom left), the thermocouple locations (right) are shown for the RTRC thin wall print.

The thin wall was measured to be 80 x 6.5 x 20.6 mm (L x W x H) and the substrate is 101.6 x 101.6 x 12.5 mm (L x W x H). The location of the thermocouples is important during FE thermal model calibration to effectively capture the temperature gradient through the substrate. The experimental data will be used to compare against the FE thermal simulation results once the proper thermal property input is determined. Although the FE simulation is overpredicting the temperature past layer five, it has good agreement in the first five layers. It was decided this was appropriate based on similar data from calibrated results from other FE modeling papers [11],

[18], [20]. The sharp peaks in the experimental data are believed to be caused either from shielding gas effects or electrical impedance from the CMT arc, but the true cause has not been determined. In future modeling efforts, the cooling rates will need to be adjusted after the first five layers most likely to have better agreement to the experimental data.

FE Thermal Model

The FE thermal simulation was built using Abaqus/Standard 2019 and the AM modeler plugin. The heat transfer found in WAAM is driven by the transient heat conduction **Equation 1** described below:

$$C_p \rho \frac{dT}{dt} = \frac{\delta}{\delta x}\left(k\frac{\delta T}{\delta x}\right) + \frac{\delta}{\delta y}\left(k\frac{\delta T}{\delta y}\right) + \frac{\delta}{\delta z}\left(k\frac{\delta T}{\delta z}\right) + q, \quad (1)$$

where C_p is the heat capacity, ρ is the material density, T is the temperature, k is the thermal conductivity, and q is the volumetric heat input. The FE thermal model uses a moving double ellipsoid Goldak heat source to simulate the arc power source [21]. The heat source includes two ellipsoidal sources that are combined to simulate the different temperature gradients at the front and rear of the melt pool. Because of this separation of front and back, the fractions f_f and f_r are used where $f_f + f_r = 2$. Goldak's equation for the power density of the front ellipsoid is listed by **Equation 2a**:

$$q(x,y,z,t) = \frac{6\sqrt{3}Pnf_f}{a_f bc\pi\sqrt{\pi}} exp\left(-3\frac{x^2}{a_f^2} - 3\frac{y^2}{b^2} - 3\frac{z^2}{c^2}\right), \quad (2a)$$

and the power density equation for the rear ellipsoid is similarly listed by **Equation 2b**:

$$q(x,y,z,t) = \frac{6\sqrt{3}Pnf_r}{a_r bc\pi\sqrt{\pi}} exp\left(-3\frac{x^2}{a_r^2} - 3\frac{y^2}{b^2} - 3\frac{z^2}{c^2}\right), \quad (2b)$$

where q(x, y, z,t) is the power density of the heat source, P is the power input, n is the efficiency of the arc, and abc are the radii in the xyz directions as referenced in Goldak's original paper [21]. The heat source model has been used in many modeling efforts and was created to simulate welding as well as metal AM [9], [11], [18], [20], [22], [23]. The double ellipsoidal parameters used for the FE thermal simulation can be found in **Table 2.**

Table 2. The Goldak heat source parameters used for the FE thermal simulation.

Factor	Symbol	Value
Efficiency	n	0.95
Half width (mm)	b	3.25
Depth (mm)	c	3.25
Front Length (mm)	af	7
Rear Length (mm)	ar	13
Front Fraction (mm)	ff	0.7
Rear Fraction (mm)	fr	1.3

The boundary conditions applied to the thermal simulation include free heat convection and thermal radiation. The surface convection coefficient applied to the part and substrate is 18 W/(m^{2}K) [24]. Radiation emissivity is held constant during the simulation being applied to the entire surface of the part and substrate with a value of 0.2 [22]. As the heat source travels along the print path, elements are progressively activated to simulate the deposited layer. Abaqus simulates the progressive addition of a material by modifying the value of its thermal conductivity: at the initial state, a very low value is assigned to the thermal conductivity of the elements prior to being activated, and then, the conductivity is increased to its actual value when the element temperature exceeds a threshold value [10]. Due to the low thermal conductivity of inactive elements, heat transfer is not able to occur

between active and inactive elements –making it appropriate to simulate material deposition. Like the actual WAAM process, the temperature increases in the inactive elements only when they are directly heated by the Goldak heat source. The mesh consists of 225,450 CD3D8 elements and can be seen in **Figure 2**.

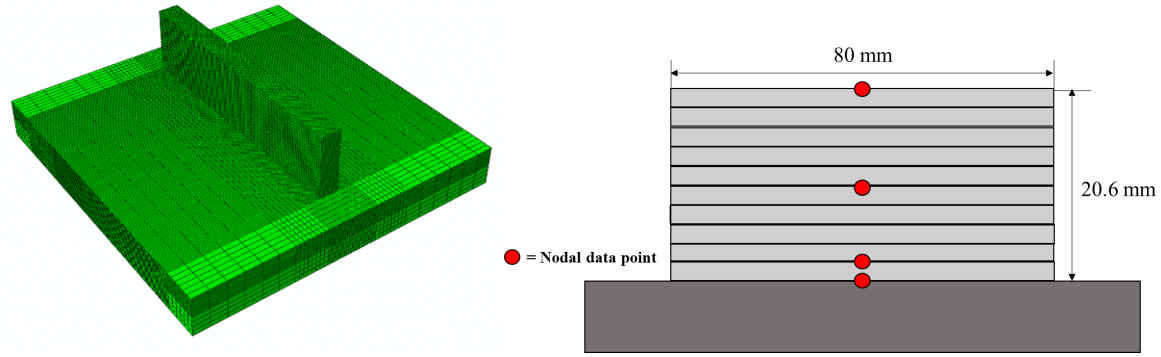

Figure 2. The FE mesh consisting of 225,450 linear brick elements (left) and the nodal extraction locations for layers 0,1,5, and 10 (right)..

FE Thermal Simulations Performed

Three variations in input thermal properties were simulated for wire and as-built M250 material in the FE thermal simulations described previously. The variations include the experimentally measured values from DSC and LFA tests, linearized values for each property, and constant values at room temperature. The measured values were input as recorded for tests "wire_exp" and "waam_exp." For the linearized properties, the first and last values were used to remove nonlinear portions for "wire_lin" and "waam_lin." Lastly, constant values at room temperature were chosen for tests "wire_RT" and "waam_RT." A description of each thermal input variation is shown in **Table 3**.

Table 3. The thermal property input details for the three test cases for each material.

Naming Convention	Material Type	Thermal Properties
wire_exp	wire	experimentally measured
waam_exp	waam	experimentally measured
wire_lin	wire	linearized properties
waam_lin	waam	linearized properities
wire_RT	wire	constant value at room temperature
waam_RT	waam	constant value at room termperature

M250 temperature dependent thermal properties were calculated for the weld wire and printed material by DSC and LFA via Netzsch and can be found in **Figure 3**. The properties for A36 were found from literature [25]. The values were measured up to a maximum temperature of 1250 °C with a heating rate of 293 °C/min.

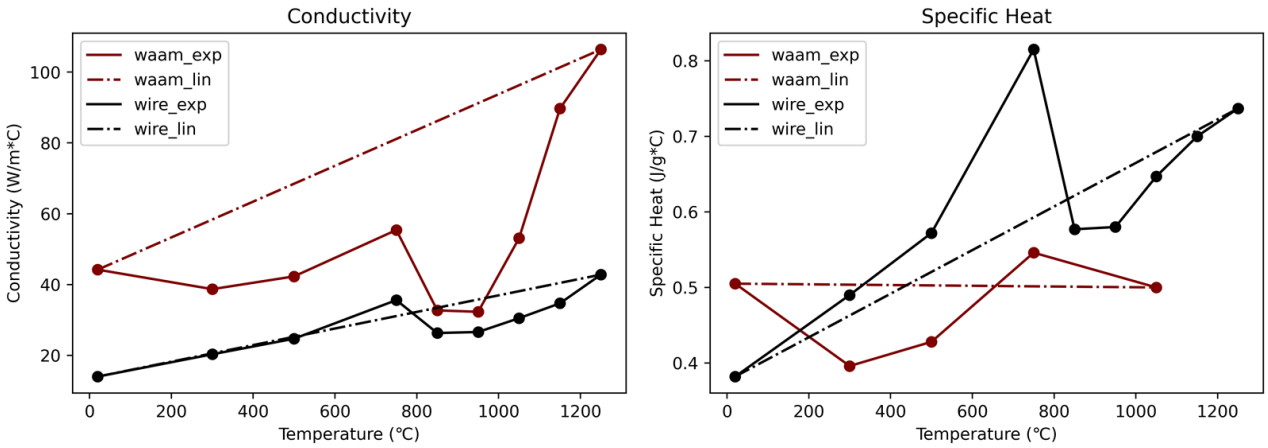

Figure 3. The measured and linearized thermal conductivity (left) and specific heat (right).

There was a slight difference in density from 7.94 to 8.48 g/cm^3 for wire and as-built material. The latent heat of fusion for M250 wire is 392.5 J/g with a solidus and liquidus temperature of 1443.5 °C and 1471.7 °C. The latent heat of fusion for the as-built M250 is 202 J/g with a solidus and liquidus temperature of 1450 °C and 1490 °C. A smoothing factor of 5 was utilized to improve convergence due to the sharp change in enthalpy in the simulation, which was also implemented in the Abaqus AM package example file [10].

Results and Discussion

The temperature history for a 10-layered thin wall built was simulated using the FE model described previously for each of the three thermal property variations for wire and as-built material. Nodal temperature was recorded at each of the thermocouple locations as well as along layers 0, 1, 5, and 10. The FE thermal history for layers 1-10 and 6-10 for thermocouple (TC0) are shown below in **Figure 4**.

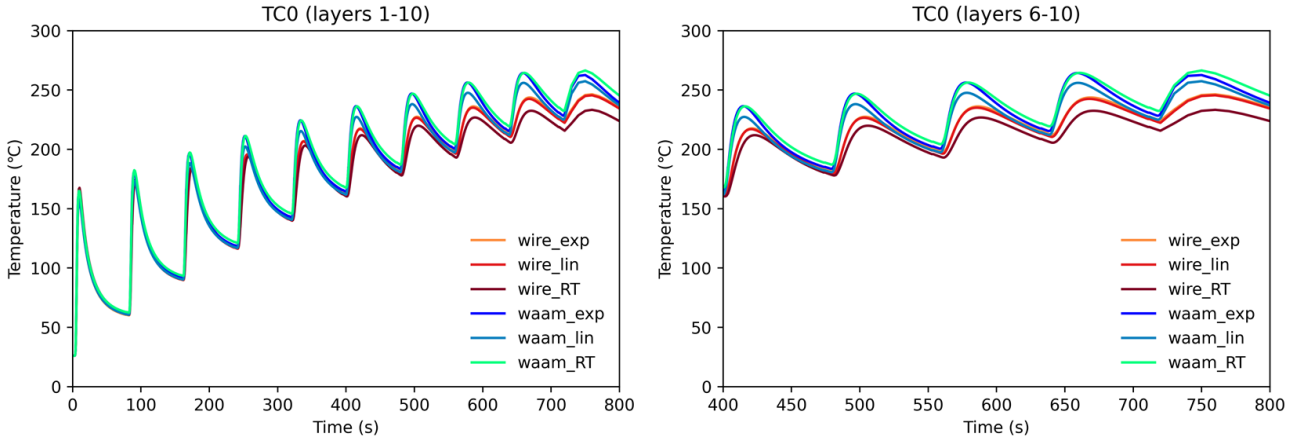

Figure 4. The FE thermal history at thermocouple TC0 for all layers (left) and layers 6-10 (right).

The nodal temperature values at the location of TC0 appear to deviate based on the thermal property input used. Considering thermocouples located on the substrate are used for calibration of the heat source parameters and boundary conditions, it is important to understand if thermal property deviation can be detected in the temperature history at these locations. On the substrate, the data shows that the constant room temperature properties for wire (wire_RT) resulted in a decrease in temperature; however, for the as-built material (waam_RT) the opposite was true. The linearized and experimental properties for the wire had the least change in temperature on the substrate compared to the other properties. For the as-built material properties, the linearized values resulted in the lowest thermal response while room temperature properties led to the highest temperatures.

To contrast the simulated temperature variations on the substrate, nodal temperature data was investigated on the part surface for layers 0, 1, 5, and 10. If large thermal variation is seen in the part, the variation in heating and cooling cycles would most likely lead to unique stress profiles that may not be detected with measurements on the substrate. The simulated thermal history for nodes centered on the build located on the top surface of layers 0, 1, 5, and 10 is shown for each thermal input variation in **Figure 5**.

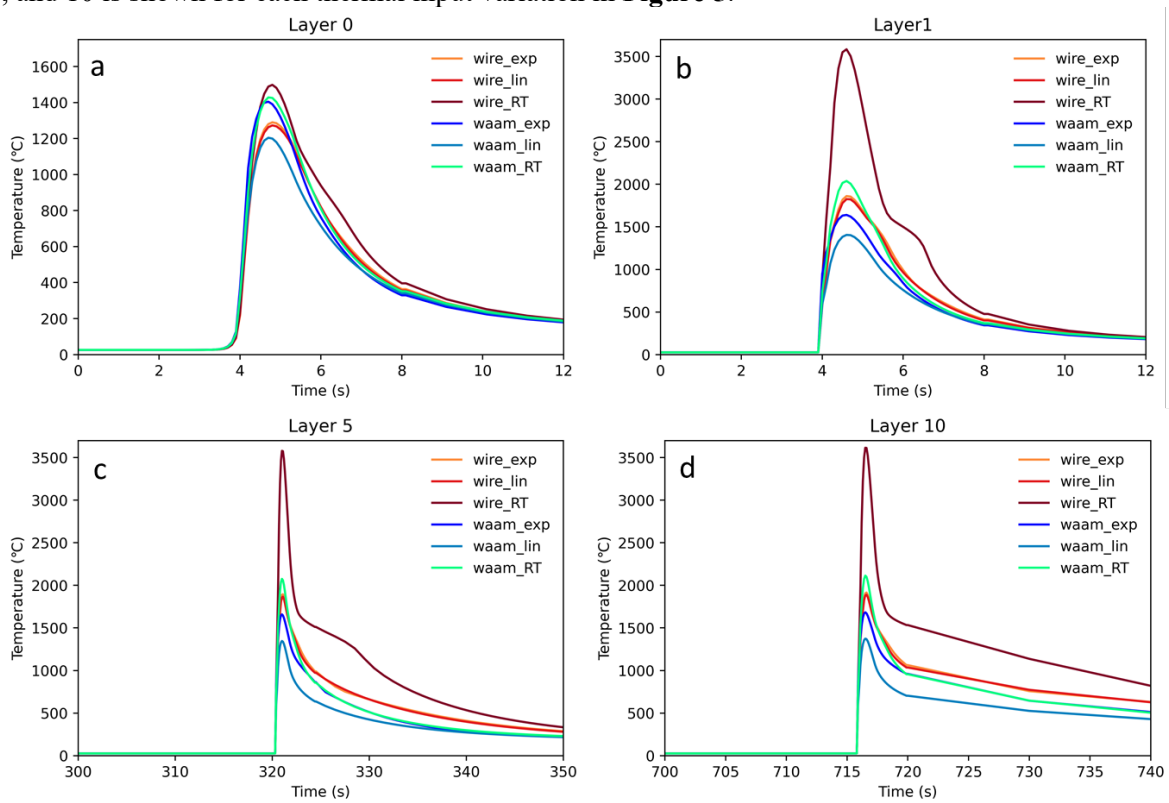

Figure 5. The FE thermal history at each nodal location for six different thermal property inputs on layer 0 (a), layer 1 (b), layer 5 (c), and layer 10 (d).

Like the temperatures measured at TC0, the values measured along several layers appear to show variation in thermal response over time for the printed layer, but the difference in temperature is much greater. The thermal history is shown to deviate substantially more in the part than along the substrate meaning the stress response would most likely deviate as well. The constant values at RT resulted in the largest temperatures for both wire and as-built material. Like the thermocouple data, the linearized and experimental values for wire material resulted in the least temperature variation of all groups tested. Overall, linearized values for both the wire and as-built material were shown to have reductions in temperature compared to the experimental and RT properties.

To understand how the melt pool may be affected by the change in thermal properties, the maximum temperature during the simulation was recorded. The values for maximum temperature are artificially high due to the few number of elements provided in the beginning of each layer. The applied volumetric heat flux is being applied to a single row of elements leading to large spikes in maximum temperature shown on the left in **Figure 6**. It is believed that following the large spikes in temperature, the value reaches a steady state temperature before cooling during each layer. This is illustrated by the plateau seen following the large spike. To better demonstrate the steady state temperatures, the maximum temperature at the selected nodes along layers 0, 1, 5, and 10 is shown on the right in **Figure 6**.

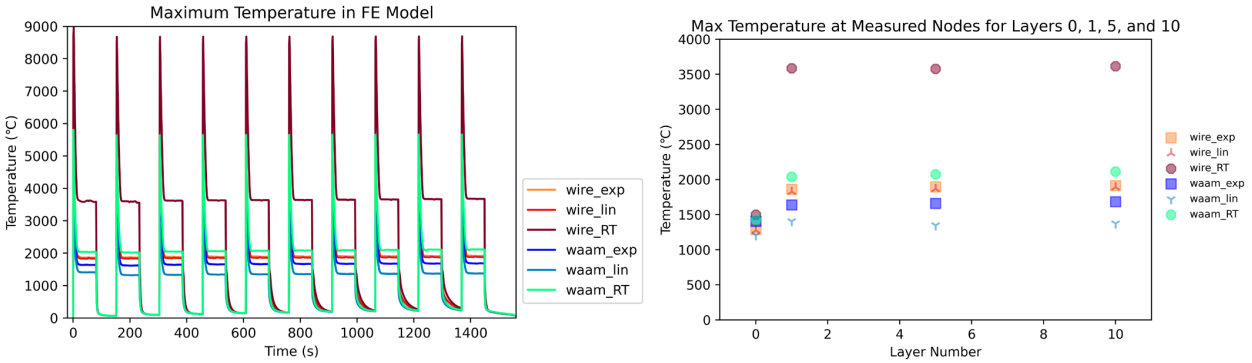

Figure 6. The maximum temperature across the entire simulation for every increment (left) and the maximum temperature recorded at each nodal location measured along the center of the part at layers 0, 1, 5, and 10 (right).

The trend for thermal variation is similar as the data previously discussed for each of the thermal input properties. The properties held constant at RT for both the wire and as-built material appear to have the largest maximum temperatures, while the linear properties had the lowest maximum temperatures for each material type. The maximum values at each of the selected nodes can be found in **Table 4**.

Table 4. Maximum temperature values for each printed material at nodal locations on layers 0, 1, 5, and 10.

	WAAM			WIRE		
Layer	**Measured (°C)**	**Linear (°C)**	**Constant (°C)**	**Measured (°C)**	**Linear (°C)**	**Constant (°C)**
0	1404	1204	1428	1290	1273	1498
1	1640	1405	2038	1861	1826	3585
5	1659	1346	2076	1895	1866	3579
10	1683	1374	2114	1915	1890	3615

The previously described trend is clear in table format —the maximum temperature values increase as the layer height increases for all thermal input properties. The trend described earlier is clear in table format. The constant values at RT for wire and as-built WAAM material were seen to have the highest maximum temperatures followed by experimentally measured properties, and linearized values.

Conclusion

FE thermal simulations of the WAAM process have been used to predict the temperature history of a 10 layered thin-wall using variations in temperature-dependent thermal properties: thermal conductivity, specific heat, and latent heat. Wire filler material and as-built WAAM printed material for M250 were collected experimentally using DSC and LFA to accurately simulate the thermal history and solidus to liquidus transition seen in the heat affected zone. The results shown suggest that the simulated thermal history can vary significantly depending on the material form selected (wire or as built), as well as the way in which the data is implemented into the thermal model. Further work needs to be performed before determining the most appropriate source for thermal properties (wrought, wire, as-built, or material database), but it can be concluded that the form of material does affect the thermal response for maraging grade 250 steel. It was shown that constant values at room temperature result in an increased thermal response for WAAM thermal simulations, and linearized properties decreased the temperature when both were compared with the experimental thermal property inputs.

Acknowledgements

This work was supported by National Center for Manufacturing Sciences (NCMS) and US Army Research Laboratory (ARL); Collaboration Agreement #202031-141054 CTMA Cooperative Agreement #HQ0034-15-2-0007.

References

[1] D. Ding, Z. Pan, D. Cuiuri, and H. Li, "Wire-feed additive manufacturing of metal components: technologies, developments and future interests," *Int J Adv Manuf Technol*, vol. 81, no. 1–4, pp. 465–481, Oct. 2015, doi: 10.1007/s00170-015-7077-3.

[2] X. Xu, "Oxide accumulation effects on wire+arc layer-by-layer additive manufacture process," p. 12, 2018.

[3] S. W. Williams, F. Martina, A. C. Addison, J. Ding, G. Pardal, and P. Colegrove, "Wire + Arc Additive Manufacturing," *Materials Science and Technology*, vol. 32, no. 7, pp. 641–647, May 2016, doi: 10.1179/1743284715Y.0000000073.

[4] K. S. Derekar, "A review of wire arc additive manufacturing and advances in wire arc additive manufacturing of aluminium," *Materials Science and Technology*, vol. 34, no. 8, pp. 895–916, May 2018, doi: 10.1080/02670836.2018.1455012.

[5] C. R. Cunningham, J. M. Flynn, A. Shokrani, V. Dhokia, and S. T. Newman, "Invited review article: Strategies and processes for high quality wire arc additive manufacturing," *Additive Manufacturing*, vol. 22, pp. 672–686, Aug. 2018, doi: 10.1016/j.addma.2018.06.020.

[6] *Additive Manufacturing Technologies*. Accessed: Jun. 08, 2022. [Online]. Available: https://link.springer.com/book/10.1007/978-1-4939-2113-3

[7] Y. Zhao, Y. Jia, S. Chen, J. Shi, and F. Li, "Process planning strategy for wire-arc additive manufacturing: Thermal behavior considerations," *Additive Manufacturing*, vol. 32, p. 100935, Mar. 2020, doi: 10.1016/j.addma.2019.100935.

[8] P. Foteinopoulos, A. Papacharalampopoulos, and P. Stavropoulos, "On thermal modeling of Additive Manufacturing processes," *CIRP Journal of Manufacturing Science and Technology*, vol. 20, pp. 66–83, Jan. 2018, doi: 10.1016/j.cirpj.2017.09.007.

[9] J. Ding, "Thermo-mechanical Analysis of Wire and Arc Additive Manufacturing Process," p. 216.

[10] P. Michaleris, "Modeling metal deposition in heat transfer analyses of additive manufacturing processes," *Finite Elements in Analysis and Design*, vol. 86, pp. 51–60, Sep. 2014, doi: 10.1016/j.finel.2014.04.003.

[11] F. Montevecchi, G. Venturini, A. Scippa, and G. Campatelli, "Finite Element Modelling of Wire-arc-additive-manufacturing Process," *Procedia CIRP*, vol. 55, pp. 109–114, Jan. 2016, doi: 10.1016/j.procir.2016.08.024.

[12] F. Hejripour, F. Binesh, M. Hebel, and D. K. Aidun, "Thermal modeling and characterization of wire arc additive manufactured duplex stainless steel," *Journal of Materials Processing Technology*, vol. 272, pp. 58–71, Oct. 2019, doi: 10.1016/j.jmatprotec.2019.05.003.

[13] L.-E. Lindgren, "Numerical modelling of welding," *Computer Methods in Applied Mechanics and Engineering*, vol. 195, no. 48, pp. 6710–6736, Oct. 2006, doi: 10.1016/j.cma.2005.08.018.

[14] N. Saunders, U. K. Z. Guo, X. Li, A. P. Miodownik, and J.-Ph. Schillé, "Using JMatPro to model materials properties and behavior," *JOM*, vol. 55, no. 12, pp. 60–65, Dec. 2003, doi: 10.1007/s11837-003-0013-2.

[15] Z. Guo, W. Sha, and D. Li, "Quantification of phase transformation kinetics of 18 wt.% Ni C250 maraging steel," *Materials Science and Engineering: A*, vol. 373, no. 1, pp. 10–20, May 2004, doi: 10.1016/j.msea.2004.01.040.

[16] R. F. D. Portergopp, "PREDICTING RESIDUAL STRESSES IN MULTI-PASS WELDMENTS WITH THE FINITE ELEMENT METHODTS," p. 14.

[17] M. Graf, A. Hälsig, K. Höfer, B. Awiszus, and P. Mayr, "Thermo-Mechanical Modelling of Wire-Arc Additive Manufacturing (WAAM) of Semi-Finished Products," *Metals*, vol. 8, no. 12, Art. no. 12, Dec. 2018, doi: 10.3390/met8121009.

[18] X. Jimenez, W. Dong, S. Paul, M. A. Klecka, and A. C. To, "Residual Stress Modeling with Phase Transformation for Wire Arc Additive Manufacturing of B91 Steel," *JOM*, vol. 72, no. 12, pp. 4178–4186, Dec. 2020, doi: 10.1007/s11837-020-04424-w.

[19] F. H. Lang and N. Kenyon, "Welding of Maraging Steels," p. 43.

[20] S. H. Lee, “CMT-Based Wire Arc Additive Manufacturing Using 316L Stainless Steel: Effect of Heat Accumulation on the Multi-Layer Deposits,” *Metals*, vol. 10, no. 2, p. 278, Feb. 2020, doi: 10.3390/met10020278.
[21] J. Goldak, A. Chakravarti, and M. Bibby, “A new finite element model for welding heat sources,” *Metall Mater Trans B*, vol. 15, no. 2, pp. 299–305, Jun. 1984, doi: 10.1007/BF02667333.
[22] E. R. Denlinger, J. Irwin, and P. Michaleris, “Thermomechanical Modeling of Additive Manufacturing Large Parts,” *Journal of Manufacturing Science and Engineering*, vol. 136, no. 6, Oct. 2014, doi: 10.1115/1.4028669.
[23] J. C. Heigel, P. Michaleris, and E. W. Reutzel, “Thermo-mechanical model development and validation of directed energy deposition additive manufacturing of Ti–6Al–4V,” *Additive Manufacturing*, vol. 5, pp. 9–19, Jan. 2015, doi: 10.1016/j.addma.2014.10.003.
[24] E. R. Denlinger, J. C. Heigel, P. Michaleris, and T. A. Palmer, “Effect of inter-layer dwell time on distortion and residual stress in additive manufacturing of titanium and nickel alloys,” *Journal of Materials Processing Technology*, vol. 215, pp. 123–131, Jan. 2015, doi: 10.1016/j.jmatprotec.2014.07.030.
[25] L. Zhang and P. Michaleris, “Investigation of Lagrangian and Eulerian finite element methods for modeling the laser forming process,” *Finite Elements in Analysis and Design*, vol. 40, no. 4, pp. 383–405, Feb. 2004, doi: 10.1016/S0168-874X(03)00069-6.